

## Structural instability and electronic excitations in Nb<sub>3</sub>Sn

B. Sadigh and V. Ozoliņš\*

Department of Theoretical Physics, Royal Institute of Technology, SE-100 44 Stockholm, Sweden

(Received 28 May 1997)

We have performed an extensive first-principles study of the cubic-to-tetragonal structural phase transformation in the A15 compound Nb<sub>3</sub>Sn, using optimized norm-conserving pseudopotentials and the plane-wave basis set. Our calculations confirm that cubic Nb<sub>3</sub>Sn is unstable with respect to the sublattice distortions of  $\Gamma_{12}$  symmetry discovered by Shirane and Axe [Phys. Rev. B **4**, 2957 (1971)]. However, the cubic phase is stable with respect to the tetragonal strain if the atoms are frozen in their ideal positions. The structural instability with respect to the sublattice distortions is explained by an unusually strong electron-phonon coupling between the  $\Gamma_{12}$  phonons and the states at the Fermi level, while no such anomalous coupling has been found for the tetragonal strain. Finite-temperature electronic-structure effects are modeled using the exact Fermi-Dirac distribution function in self-consistent local-density-approximation calculations. Electronic excitations are found to stabilize the cubic phase above  $T_M=450$  K. The model correctly reproduces several experimental findings, including the softening of the elastic constant  $C'$  and zone-center optical  $\Gamma_{12}$  frequency  $\nu_{\Gamma_{12}}$  as  $T \rightarrow T_M$ , as well as their subsequent stiffening below  $T_M$ . Furthermore,  $C'$  is found to approach zero at  $T_M$ , while  $\nu_{\Gamma_{12}}$  does not, which is again consistent with the observed behavior of Nb<sub>3</sub>Sn. [S0163-1829(98)05105-4]

### I. INTRODUCTION

Metallic systems are known to exhibit interesting structural and phonon anomalies associated with certain unusual features of the electronic structure (e.g., Fermi-surface nesting, strong electron-phonon interactions, Kohn anomalies). Furthermore, in contrast to insulating systems such as ferroelectrics, where the structural transitions are driven by vibrational excitations, the nonexistence of the gap in the electronic excitation spectrum offers the intriguing possibility of electronic excitations stabilizing phases which are otherwise unstable at  $T=0$  K. A necessary prerequisite for this stabilization is a profound change in the electronic structure with the structural transformation, which manifests itself as an anomalously strong temperature dependence in properties that are normally temperature independent. Nb<sub>3</sub>Sn, belonging to the group of A<sub>3</sub>B intermetallic compounds with the A15 or  $\beta$ -tungsten structure, is known to exhibit such anomalies in the electric, magnetic, elastic, and structural properties. Much research was focused on the study of A15 compounds during the 1960's and 1970's because of their relatively high superconducting transition temperatures ( $T_c \approx 18$  K for Nb<sub>3</sub>Sn). The review articles by Testardi,<sup>1</sup> Weger and Goldberg,<sup>2</sup> and Allen<sup>3</sup> summarize the status of two decades of experimental and theoretical effort in this area.

The A15 (or  $\beta$ -W) structure (cubic space group  $Pm\bar{3}n$ ) is shown in Fig. 1. Soon after the discovery of their high superconductivity temperatures, structural instabilities were observed in many A15 compounds. The reported measurements were done by Batterman and Barrett<sup>4</sup> on V<sub>3</sub>Si. Later, Mailfert *et al.*<sup>5</sup> found that Nb<sub>3</sub>Sn below  $T_M=43$  K undergoes a martensitic transition from the cubic A15 to a tetragonal phase. The proximity of this and the superconducting transition temperature  $T_c$  suggests a possible relation between the structural instability and superconductivity in

Nb<sub>3</sub>Sn. The strain parameter of the low- $T$  phase,  $\epsilon \equiv c/a - 1$ , was measured to be  $-0.0062$ . Keller and Hanak<sup>6</sup> showed that the elastic constant  $C' = \frac{1}{2}(C_{11} - C_{12})$  softens with decreasing temperature and approaches zero at the martensitic transition temperature  $T_M$ . Thus, the Batterman-Barrett instability appears to be a "soft-mode" phase transition driven by long-wavelength (acoustic) instability.

The early measurements by Batterman and Barrett<sup>4</sup> indicated the occurrence of a second-order transition. Using phenomenological Landau theory, Anderson and Blount<sup>7</sup> found that a transition with strain as the primary order parameter would be first order with a discontinuity in  $\epsilon(T)$  and  $C_{11} - C_{12}$  behaving as  $T - T_M$  for temperatures above  $T_M$ . In an attempt to reconcile their findings with the existing experimental data,<sup>4</sup> Anderson and Blount proposed the existence of a hidden "primary" order parameter (e.g., a sublattice distortion), which couples to the strain through a higher ( $n > 2$ ) order term in the Hamiltonian and causes a second-order transition with no discontinuity in  $\epsilon(T)$ . Shirane and

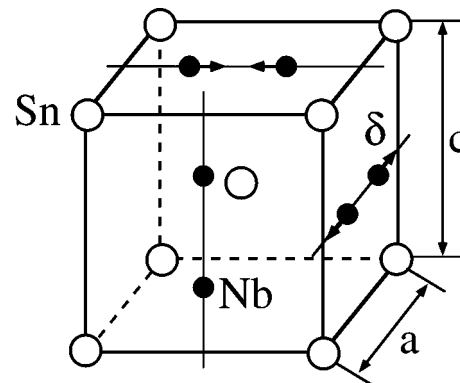


FIG. 1. The A15 structure. It contains eight atoms in a simple cubic unit cell. The Sn atoms occupy the bcc sites in the unit cell, while two Nb atoms are located on each face of the cube, half-way displaced from the center of the cube face towards the edges.

Axe<sup>8</sup> later found a sublattice distortion in Nb<sub>3</sub>Sn, corresponding to a frozen-in optical phonon with  $\Gamma_{12}$  symmetry. It could be characterized by a displacement parameter  $\delta$  which is the fraction of the pairing of the Nb atoms along the two chains orthogonal to the tetragonal axis (see Fig. 1). Neutron<sup>8</sup> and x-ray<sup>9</sup> measurements have determined that  $\delta$  and  $\epsilon$  have the same sign in Nb<sub>3</sub>Sn, and  $\delta \approx -0.0032$ . This sublattice distortion does not satisfy the criteria of Anderson and Blount<sup>7</sup> for a second-order transition since it has the same tetragonal symmetry as the strain, which allows for bilinear coupling between them (of type  $A_1 \delta \epsilon$ ) and still leads to a first-order transition. However, more accurate measurements had already shown that the transition in Nb<sub>3</sub>Sn is in fact first order with a small discontinuity in  $\epsilon(T)$ ,<sup>5</sup> and that  $C_{11} - C_{12}$  behaves as  $T - T_M$  for temperatures above  $T_M$ ,<sup>10</sup> in agreement with the results of thermodynamic analysis.<sup>7</sup>

There have been numerous attempts to explain the anomalous properties of A15 compounds either by their unusual electronic structure<sup>11-15</sup> or by strongly anharmonic lattice vibrations.<sup>16</sup> Several authors<sup>17-22</sup> have considered the band structure of various A15 compounds, but the severe computational cost has prevented extensive and accurate *ab initio* total-energy calculations mapping out the energy surface underlying the cubic-to-tetragonal structural transition. It has been shown<sup>17-22</sup> that the electronic band structures of A15 compounds are very similar, suggesting that the anomalous behavior is caused by similar physical mechanisms. In this work we concentrate on one particular A15 compound, namely Nb<sub>3</sub>Sn, which we study in detail. Through self-consistent total-energy and electronic free-energy calculations, we investigate the nature of the transition and demonstrate the importance of electronic excitations for the relative stabilities of the cubic and tetragonal phases at  $T > 0$ .

The paper is organized as follows. Section II contains a description of the computational details. Section III gives an account of our  $T = 0$  results for the energy surface as a function of the two distortion parameters  $\delta$  and  $\epsilon$ . Finite-temperature and electronic excitation effects are described in Sec. IV where it is shown that the cubic phase of Nb<sub>3</sub>Sn is stabilized by the electronic free energy. Finally, we conclude with a discussion in Sec. V.

## II. METHOD

### A. $T = 0$ calculations

The electronic band structure is calculated within the local-density approximation (LDA) of the density-functional theory,<sup>23</sup> using the Perdew-Zunger<sup>24</sup> parametrization of the Ceperley-Alder<sup>25</sup> results for the exchange-correlation functional. The electron-ion interaction is represented by separable norm-conserving pseudopotentials,<sup>26</sup> generated to treat the extended  $4s$  and  $4p$  semicore states of Nb as valence, on equal footing with the  $5s$ ,  $5p$ , and  $4d$  states. This treatment has the additional advantage of eliminating the need for the nonlinear core correction,<sup>27</sup> and has been found to produce accurate pseudopotentials for all early transition metals.<sup>28</sup> The optimization technique of Ref. 29 is employed to reduce the required plane-wave cutoff to a manageable  $E_{\text{cut}} = 40$  Ry, which amounts to approximately 4200 plane waves per wave function at the equilibrium volume. We use the conjugate

gradient method to solve iteratively the Schrödinger equation and the modified Broyden mixing scheme to achieve the potential self-consistency.

Particular attention has been paid to the accuracy of the Brillouin-zone summations. Most special-points methods use artificial thermal broadening<sup>30-32</sup> to reduce the required number of  $\mathbf{k}$  points. Such a procedure complicates the definition of temperature for the electronic subsystem and introduces an unphysical dependence of the calculated total energy on the chosen broadening width. Since we intend to study effects of finite temperature and electronic excitations, we need a method which treats the  $T = 0$  and  $T > 0$  cases consistently. Therefore, the corrected tetrahedron method of Blöchl, Jepsen, and Andersen<sup>33</sup> has been selected for the present study. We have chosen a  $14 \times 14 \times 14$  mesh, yielding 196 points in the irreducible part of the tetragonal Brillouin zone. Several tests have been performed with a higher ( $E_{\text{cut}} = 50$  Ry) plane-wave cutoff and a  $20 \times 20 \times 20$   $\mathbf{k}$  point mesh, showing that the total-energy differences are very well converged with respect to these parameters.

We obtain the equilibrium lattice constant  $a_{\text{calc}} = 5.257$  Å, to be compared with the experimental value<sup>34</sup>  $a_{\text{exp}} = 5.292$  Å. All calculations in this work are performed at the theoretical zero pressure volume  $V_0 = a_{\text{calc}}^3$ . Distortion energies are studied by freezing-in the sublattice distortion  $\delta$  and tetragonal strain  $\epsilon$ , and taking the energy difference:

$$\Delta E^{\text{LDA}}(\epsilon, \delta) = E_{\text{tot}}(\epsilon, \delta) - E_{\text{tot}}^{\text{cubic}}, \quad (1)$$

where  $E_{\text{tot}}^{\text{cubic}}$  is the energy of the cubic phase.  $\Delta E^{\text{LDA}}(\epsilon, \delta)$  has been computed for pairs of  $(\delta, \epsilon)$  on a regular grid of values  $|\epsilon| \leq 0.02$  and  $|\delta| \leq 0.01$ .

### B. $T > 0$ calculations

Our finite-temperature calculations are performed with the electronic occupation numbers obtained from the Fermi-Dirac distribution. These occupation numbers are used in the self-consistency process to obtain the charge density and total energy. In practice, it is done by integrating the zero-temperature results for various Fermi energies, weighted with the energy derivative of the distribution function  $f((\epsilon - \epsilon_F)/k_B T)$ :

$$\rho(T) = - \int d\epsilon \epsilon'_F f' \left( \frac{\epsilon'_F - \epsilon_F}{k_B T} \right) \int_{-\infty}^{\epsilon'_F} \rho(\epsilon) d\epsilon, \quad (2)$$

where  $\epsilon_F$  is the actual Fermi energy and  $\rho(\epsilon)$  is a sum over all electronic states,  $\rho(\epsilon) = \sum_i \delta(\epsilon - \epsilon_i) \rho_i$  (everywhere in this section  $\epsilon$  is the energy, not the tetragonal distortion). The second integral in Eq. (2) is calculated using the corrected tetrahedron method, while the first integration can be conveniently carried out by averaging the occupation numbers of the tetrahedron method<sup>33</sup> for different positions of the Fermi level.

The electronic entropy is calculated from the density-of-states  $N(\epsilon, T)$  using the standard expression for the noninteracting electron gas:<sup>35</sup>

$$S_{\text{el}}(T) = -k_B \int_{-\infty}^{\infty} d\epsilon N(\epsilon, T) [f(x) \ln f(x) + (1-f(x)) \ln(1-f(x))], \quad (3)$$

where  $x = (\epsilon - \epsilon_F)/k_B T$ . The free energy, including the electronic entropy of Eq. (3), is

$$F(T) = E_{\text{tot}}(T) - TS_{\text{el}}(T). \quad (4)$$

At ambient temperatures the following expressions hold for the electronic entropy  $S(T)$ , total energy  $E_{\text{tot}}(T)$ , and free energy  $F(T)$ :

$$S(T) = \gamma T, \quad (5)$$

$$E_{\text{tot}}(T) = E_{\text{tot}}(T)|_{T=0} + \frac{\gamma}{2} (k_B T)^2, \quad (6)$$

$$F(T) = E_{\text{tot}}(T)|_{T=0} - \frac{\gamma}{2} (k_B T)^2, \quad (7)$$

where  $\gamma$  is the linear coefficient of the low- $T$  electronic specific heat. The low-temperature Sommerfeld expansion<sup>36</sup> gives

$$\gamma = \frac{\pi^2}{3} N(\epsilon_F), \quad (8)$$

where  $N(\epsilon_F)$  is the density of the states at the Fermi level. Equation (8) shows that the electronic excitations favor phases with high  $N(\epsilon_F)$ . However, the Sommerfeld expansion may fail even for fairly low temperatures and therefore it is not used to obtain the results of this work. Instead, we calculate  $F(T)$  self-consistently at two different temperatures using Eqs. (3) and (4), and then extract  $\gamma$  with the help of Eq. (7).

### III. STRUCTURAL INSTABILITY OF THE CUBIC PHASE AT $T=0$

#### A. $T=0$ energy

The calculated deformation energy of  $\text{Nb}_3\text{Sn}$  as a function of the tetragonal shear  $\epsilon$  and sublattice distortion  $\delta$  is shown in Fig. 2. This figure is obtained by fitting the directly calculated total-energy differences  $\Delta E^{\text{LDA}}(\epsilon, \delta)$  of Eq. (1) with the following functional form:

$$\Delta E(\epsilon, \delta) = E_0(\delta) + \frac{1}{2} C'(\delta) [\epsilon - \epsilon_0(\delta)]^2. \quad (9)$$

Here  $E_0(\delta)$ ,  $C'(\delta)$ , and  $\epsilon_0(\delta)$  are 8th degree polynomial functions of the sublattice distortion  $\delta$ . The cubic symmetry of the undistorted A15 structure (corresponding to  $\epsilon = \delta = 0$ ) requires that the coefficients of the first-order term in  $E_0(\delta)$  and of the zeroth-order term in  $\epsilon_0(\delta)$  are both zero. The functions  $E_0(\delta)$ ,  $C'(\delta)$ , and  $\epsilon_0(\delta)$  have a simple physical interpretation: If the sublattice distortion is fixed to a certain value  $\delta_0$  and the crystal is allowed to relax by spontaneous tetragonal strain, then  $E_0(\delta_0)$  is the strain energy,  $C'(\delta_0)$  is the tetragonal elastic constant  $\frac{1}{2}(C_{11} - C_{12})$ , and  $\epsilon_0(\delta_0)$  is the equilibrium tetragonal strain. The quality of the fit using Eq. (9) is found to be very good, with maximum

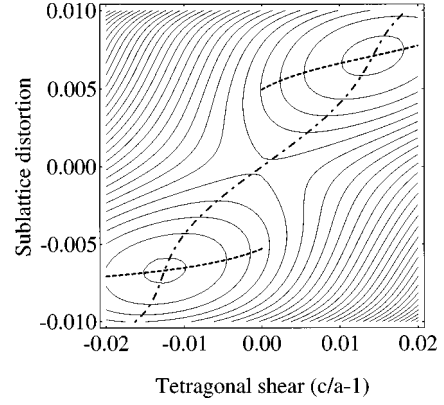


FIG. 2. Contour plot of the calculated  $T=0$  distortion energy  $\Delta E(\epsilon, \delta)$ . Locally stable minima are located at  $(\epsilon = -0.012, \delta = -0.006)$  and  $(\epsilon = +0.014, \delta = +0.007)$ , while the cubic phase corresponds to a saddle point unstable with respect to the sublattice distortion  $\delta$ . The dashed lines show the stable branches of  $\delta_0(\epsilon)$  obtained from Eq. (10), and the dot-dashed line shows  $\epsilon_0(\delta)$  in Eq. (9).

deviations between the directly calculated and fitted energies being less than 1 meV/cell. An interesting feature of Eq. (9) is that it is strictly harmonic with respect to the tetragonal shear  $\epsilon$  for any fixed distortion  $\delta$ . Furthermore, the tetragonal shear and lattice distortion couple in the first order through a term with  $\epsilon\delta$ , showing that a nonzero value of one causes a generalized force on the other. In other words, tetragonal strain  $\epsilon \neq 0$  leads to nonzero atomic forces, and finite  $\delta$  gives rise to a tetragonal stress field.

The total-energy surface  $\Delta E(\epsilon, \delta)$  in Fig. 2 has two minima: one at  $(\epsilon < 0, \delta < 0)$  and the other at  $(\epsilon > 0, \delta > 0)$ . The undistorted cubic structure with  $(\epsilon = 0, \delta = 0)$ , located at the center of the plot, is not an energy minimum but a saddle point (maximum with respect to  $\delta$ , minimum with respect to  $\epsilon$ ). Thus, the cubic phase of  $\text{Nb}_3\text{Sn}$  is unstable at  $T=0$  with respect to a spontaneous sublattice distortion. This distortion lowers the crystal symmetry and induces tetragonal strain via the  $\epsilon\delta$  term implicit in Eq. (9). For a better understanding of the energy surface in Fig. 2 we have marked two lines, each describing a different way of minimizing  $\Delta E(\epsilon, \delta)$ . The dashed lines show the relation  $\delta_0(\epsilon)$  implicitly determined by the following condition:

$$\left. \frac{\partial}{\partial \delta} \Delta E(\epsilon, \delta) \right|_{\delta = \delta_0} = 0, \quad (10)$$

which describes the equilibrium value of  $\delta$  under a fixed tetragonal shear  $\epsilon$ . It can be obtained from standard LDA total-energy calculations<sup>37</sup> by fixing the  $c/a$  ratio and relaxing the atomic positions using the Hellmann-Feynman forces. The dash-dotted line is the function  $\epsilon_0(\delta)$  in Eq. (9), which is the solution of

$$\left. \frac{\partial}{\partial \epsilon} \Delta E(\epsilon, \delta) \right|_{\epsilon = \epsilon_0} = 0. \quad (11)$$

It can also be calculated directly from the LDA by fixing  $\delta$  and optimizing the  $c/a$  ratio. These quantities exhibit remarkably different behavior;  $\epsilon_0(\delta)$  is continuous and passes

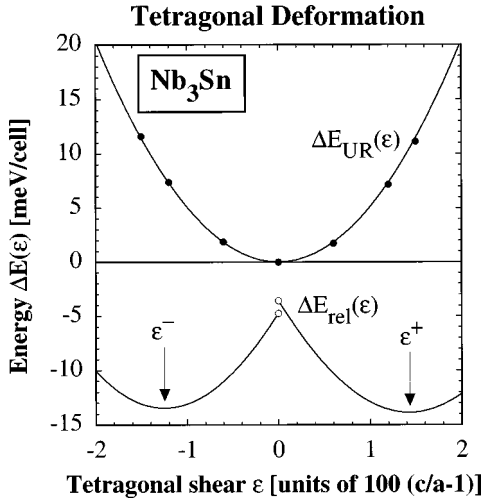


FIG. 3. The deformation energy of  $\text{Nb}_3\text{Sn}$  as a function of the tetragonal shear  $\epsilon$ . The top curve [marked  $\Delta E_{\text{UR}}(\epsilon)$ ] is obtained from  $\Delta E(\epsilon, \delta=0)$  and corresponds to the “unrelaxed”  $\delta$ . The bottom curves are calculated from  $\Delta E_{\text{rel}}(\epsilon) = \min_{\delta} \Delta E(\epsilon, \delta)$ . The filled circles are directly calculated LDA values and the empty circles show the limiting values at  $\epsilon=0$  for both branches of  $\delta_0(\epsilon)$  from Fig. 2.

through the cubic phase, while  $\delta_0(\epsilon)$  is discontinuous at  $\epsilon=0$  and is never zero (we exclude the special solution  $\epsilon = \delta=0$  since it does not describe a locally stable state if  $\delta$  is not fixed). This discontinuity is another reflection of the instability of the cubic phase, i.e., *even at  $\epsilon=0$  the crystal will spontaneously distort to  $\delta \neq 0$ .*

Figure 3 shows the deformation energy of  $\text{Nb}_3\text{Sn}$  as a function of the tetragonal shear. The upper curve (unrelaxed or “UR”) is obtained by straining the crystal tetragonally without relaxing the cell-internal coordinate  $\delta$ . Points represent the directly calculated LDA deformation energies, Eq. (1). It is seen that there is no instability in this case. The bottom curves are obtained by minimizing the total energy with respect to the cell-internal degree of freedom  $\delta$  for each shear  $\epsilon$ , showing the total energy along the dashed  $\delta_0(\epsilon)$  lines in Fig. 2. Since the  $\delta_0(\epsilon)$  curve has two branches, there are two distinct limiting values of  $\Delta E_{\text{rel}}(\epsilon)$  as  $\epsilon \rightarrow \pm 0$ . Both these values are negative, showing that the cubic phase is unstable. Since the sublattice distortion  $\delta$  corresponds to an optical phonon of  $\Gamma_{12}$  symmetry, we conclude that the cubic phase at  $T=0$  exhibits phonon instabilities.

The relaxed deformation energy  $\Delta E_{\text{rel}}(\epsilon)$  has two local minima, marked by  $\epsilon^+$  and  $\epsilon^-$  in Fig. 3 and located around the  $c/a$  values 0.988 and 1.014. The minimum at  $c/a = 1.014$  is insignificantly deeper than the minimum at  $c/a = 0.988$ . This energy difference is less than 0.5 meV/cell, far below the accuracy that is usually expected from the LDA. Experimentally, the low-temperature values of  $c/a$  range from 0.9938 to 0.9964, depending on the sample, and in many cases the cubic-to-tetragonal transition is suppressed by lattice defects. Our calculated strain on the negative  $\epsilon$  side  $c/a = 0.988$  is larger than what is seen experimentally, but sample imperfections may account for part of the discrepancy. Figure 3 can be directly compared to Fig. 3 in Lu and Klein.<sup>37</sup> The agreement between the predicted distortion energies is very good, although they obtain a slightly different

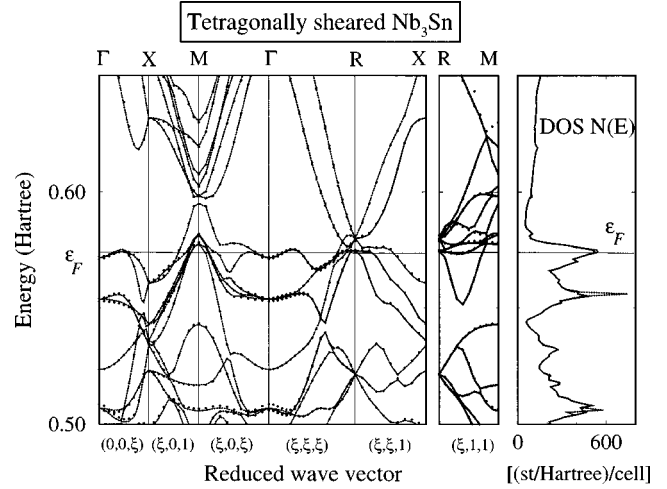


FIG. 4. Electronic band structure of tetragonally sheared  $\text{Nb}_3\text{Sn}$  with ( $\epsilon=0.075$ ,  $\delta=0$ ). The bands of the cubic and tetragonal crystal are marked by dotted lines and dots, correspondingly. The density of states curve of the distorted crystal is given as continuous line.

equilibrium value of  $c/a$  and find that the global minimum of  $\Delta E_{\text{rel}}(\epsilon)$  is on the negative  $\epsilon$  side. However, their calculated energy difference  $\Delta E(\epsilon^+) - \Delta E(\epsilon^-)$  is also extremely small, and Lu and Klein note that the flatness of the  $\Delta E_{\text{rel}}(\epsilon)$  curve complicates an accurate determination of the equilibrium  $c/a$  value. Both studies agree on the essential aspect that at  $T=0$  K the cubic  $\text{Nb}_3\text{Sn}$  phase is dynamically unstable.

## B. Electronic structure of $\text{Nb}_3\text{Sn}$

Several microscopic theories<sup>11–15</sup> have attempted to explain the unusual properties of A15 compounds in terms of their electronic structure. The most realistic of these theories identify the source of anomalies in the unique occurrence of a sixfold degeneracy at the  $R$  point of the Brillouin zone and a singularity in the density-of-states near the Fermi level. The difficulty with such models has been their focusing on a small part of the Brillouin zone. Mattheiss and Weber<sup>22</sup> performed a very thorough study of the band structure of  $\text{Nb}_3\text{Sn}$ , using the nonorthogonal tight-binding method, and found that tetragonal distortions cause a splitting of flat portions of the cubic  $\Gamma_{12}$  subbands near  $\epsilon_F$ , producing substantial changes in the shape and topology of the Fermi surface. They suggested that this splitting pushes one of the bands above and the other below the Fermi energy, thus lowering the band-structure energy.

It is interesting to see if the earlier theories are confirmed by state-of-the-art electronic-structure calculations. In what follows, the structural instability of cubic  $\text{Nb}_3\text{Sn}$  is analyzed in terms of the electronic response to the structural distortions. Figures 4 and 5 show the self-consistently calculated LDA energy band structure of  $\text{Nb}_3\text{Sn}$  subject to a tetragonal shear ( $\epsilon=0.075$ ,  $\delta=0$ ) and sublattice distortion ( $\epsilon=0$ ,  $\delta=0.005$ ), correspondingly. The energy bands of the cubic crystal are shown as dotted lines, the points represent the levels of the distorted crystal, the dashed and the continuous lines in the density-of-states (DOS) panels are the electronic DOS of the cubic and distorted phases. The Fermi level,

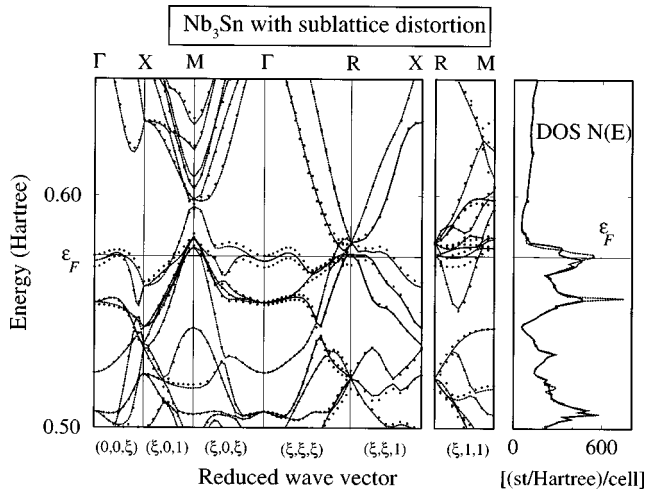


FIG. 5. The same as Fig. 4, but for a crystal with sublattice distortion ( $\epsilon=0$ ,  $\delta=0.005$ ).

which is almost unaffected by these distortions, is marked as a continuous horizontal line at  $\epsilon_F=0.574$  Hartree. Several important observations can be made from Figs. 4 and 5.

(i) The Fermi level of the cubic phase falls on a sharp peak in the electronic DOS, with a value per cell of  $N(\epsilon_F) \approx 500$  states/Hartree. This peak is caused by flat, nearly dispersionless bands at  $\epsilon_F$ , seen in Fig. 4 in the  $\Gamma-X$ ,  $\Gamma-R$ , and  $R-M$  directions. A *fourfold* degenerate  $R$  state is only a few meV above the Fermi level, while the sixfold degenerate  $R$  state is 1.4 eV below  $\epsilon_F$ .

(ii) Pure tetragonal shear (see Fig. 4) does not affect the electronic structure in any anomalous way. In fact, the energy bands of the distorted and undistorted crystal are nearly the same, showing no appreciable splitting of the cubic bands at the Fermi level. The DOS curve of the strained crystal is not affected either. Therefore, we conclude that theories which attempt to explain the anomalous properties of  $\text{Nb}_3\text{Sn}$  on the basis of band splitting under macroscopic tetragonal strain do not capture the relevant physics.

(iii) Figure 5 shows that the sublattice distortion (corresponding to a  $\Gamma_{12}$  optical phonon) has a remarkably strong influence on the bands at the Fermi level, while most of the states below  $\epsilon_F$  are affected very little (the dots fall on the dashed lines below  $\epsilon_F$  in Fig. 5). The flat bands between  $\Gamma$  and  $X$ ,  $\Gamma$  and  $R$ , and at the  $R$  point are split by a huge amount, many states move below the Fermi level, while the unoccupied states move further away from  $\epsilon_F$ . The fourfold degenerate state above the Fermi level at the  $R$  point is split in a proportion 2:2. The sharp peak of the cubic DOS is also split into two, one above and one below the Fermi energy. The density of states at the Fermi level,  $N(\epsilon_F)$ , is reduced by 25% to below 400 states/Hartree. These large splittings are indicative of a strong electron-phonon coupling between the  $\Gamma_{12}$  optical phonon and states at the Fermi level, which is probably also responsible for the relatively high superconducting  $T_c$  of this compound.

We conclude that the instability of cubic  $\text{Nb}_3\text{Sn}$  is caused by a simultaneous presence of two factors: flat degenerate bands at the Fermi level and unusually large shifts in their energies upon the phonon distortion of  $\Gamma_{12}$  symmetry. It is hard to single out one particular region of the Brillouin zone

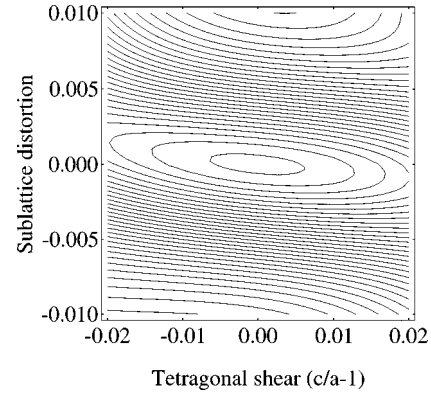


FIG. 6. Contour plot of the function  $\gamma(\epsilon, \delta)$  describing the electronic excitations in Eq. (7). The maximum is attained in the cubic phase with ( $\epsilon=0$ ,  $\delta=0$ ).

which could be ‘‘blamed’’ for the instability, since we find that the states at  $\epsilon_F$  throughout the Brillouin zone contribute rather democratically. It is tempting to speculate that both the structural instability and high superconducting  $T_c$  of  $\text{Nb}_3\text{Sn}$  are manifestations of the same physical phenomenon—strong electron-phonon interaction.

#### IV. STABILIZATION OF THE CUBIC PHASE AT FINITE TEMPERATURES

The abrupt changes in the  $T=0$  electronic structure induced by the sublattice distortion  $\delta$  (cf. Sec. III B) suggest that the electronic excitations may change the behavior at elevated temperatures. Indeed, the electronic free energy in the low-temperature limit is given by Eq. (7), where  $\gamma$  is roughly proportional to the density of states at the Fermi level, Eq. (8). Since the value of  $N(\epsilon_F)$  is highest in the cubic phase and decreases with increasing distortion, it is possible that the cubic phase is stabilized by electronic excitations at some  $T>0$ .

These considerations motivate a finite-temperature study of the electronic free energy of  $\text{Nb}_3\text{Sn}$ . We have performed self-consistent calculations using the Fermi-Dirac occupation function for the electronic system, as described in Sec. II B. Lattice vibrations are not included, but their likely effects are briefly discussed in Sec. V. The free-energy functional  $F(T, \epsilon, \delta)$  is calculated directly from the LDA at  $T=158$  K and  $T=316$  K using Eqs. (3) and (4), and then fitted with the low-temperature form Eq. (7) to obtain  $\gamma(\epsilon, \delta)$ . Since the temperatures considered are very low compared to  $\epsilon_F$ , no accuracy is lost by using Eq. (7) instead of the formally exact but somewhat inconvenient Eq. (4).

In Fig. 6 we show the contour plot of  $\gamma(\epsilon, \delta)$ . The global maximum of  $\gamma(\epsilon, \delta)$ , occurs at ( $\epsilon=0$ ,  $\delta=0$ ) indicating that the cubic phase is indeed favored by the electronic excitations. We also point out that  $\gamma$  is a rapidly varying function of the sublattice distortion  $\delta$ , and a slowly varying function of the tetragonal shear  $\epsilon$ . This is completely consistent with the results of Sec. III B where it is found that  $\delta$  causes large changes in the band structure at the Fermi level, while  $\epsilon$  does not.

Figure 7 shows the relaxed free energy of tetragonal distortion  $\Delta F_{\text{rel}}(\epsilon, T)$  at four different temperatures. Each  $\Delta F_{\text{rel}}(\epsilon, T)$  curve is obtained by relaxing the cell-internal

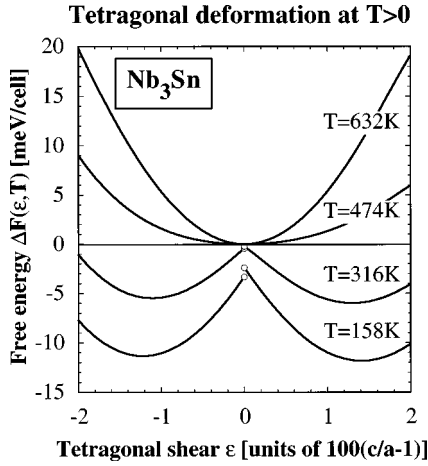


FIG. 7. The relaxed free energy as a function of the tetragonal shear at four different temperatures. Empty circles are the limiting values at  $\epsilon=0$  for sublattice distortions with  $\delta>0$  and  $\delta<0$ .

coordinate  $\delta$  to its equilibrium value, in the same fashion as for the  $\Delta E_{\text{rel}}(\epsilon)$  curves in Fig. 3. The free energy  $\Delta F_{\text{rel}}(\epsilon, T)$  at  $T=632$  K is non-negative and very harmonic, showing that at this temperature the cubic phase is completely stable with respect to all considered distortions. The temperature dependence of the elastic constant  $C'(T)$  is calculated from the curvature of the free-energy curves of Fig. 7 at the equilibrium values  $\epsilon_0(T)$  (which are nonzero below the transition point). It would be incorrect to calculate  $C'(T)$  by differentiating the electronic free energy twice with respect to the strain,

$$C'(T) \neq \frac{1}{3} \left. \frac{\partial^2}{\partial \epsilon^2} F(\epsilon, \delta, T) \right|_0, \quad (12)$$

since cell-internal relaxations would be completely neglected by this treatment. Furthermore, it would give incorrect results for cubic  $\text{Nb}_3\text{Sn}$ . Indeed, Fig. 6 shows that  $\gamma$  varies slowly with  $\epsilon$ , and Eq. (9) gives that the  $T=0$  deformation energy  $\Delta E$  is a non-negative harmonic function of  $\epsilon$ . Therefore, one would obtain an almost  $T$ -independent elastic constant  $C'(T)$ , which would counter with the experimental fact that  $C'$  shows a pronounced softening above the transition.<sup>6,38</sup> The correct procedure is to assume that the sublattice distortions occur on a fast time scale and follow the strain adiabatically,<sup>3</sup> minimizing the free energy for each  $\epsilon$ . Then one can show that

$$C'(T) = \frac{1}{3} \left( F_{\epsilon, \epsilon}(\epsilon, \delta, T) - \frac{F_{\epsilon, \delta}^2(\epsilon, \delta, T)}{F_{\delta, \delta}(\epsilon, \delta, T)} \right) \Big|_0, \quad (13)$$

evaluated at  $\epsilon$  and  $\delta$  which minimize the free energy  $F(\epsilon, \delta, T)$ . The calculated elastic constant  $C' = \frac{1}{2}(C_{11} - C_{12})$  at  $T=632$  K is 0.82 Mbar, which is close to the experimental room-temperature value  $\approx 0.7$  Mbar. It is very surprising that such a dramatic change in the elastic constant of the cubic phase (from  $C' < 0$  to  $C' = 0.82$  Mbar) can be caused by electronic excitations due to a seemingly insignificant (on the electronic energy scale) temperature increase from  $T=0$  K to  $T=632$  K.

As the temperature is lowered, the free-energy curve in Fig. 7 becomes flatter around  $\epsilon=0$ , corresponding to a softening shear elastic constant  $C'(T)$ , and already at  $T=316$  K there are two distinct minima in  $\Delta F_{\text{rel}}(\epsilon, T)$ . The spontaneous energy lowering at  $\epsilon=0$  due to the sublattice distortion  $\delta$  (represented by open circles on the  $T=316$  K curve in Fig. 7) is very small at this temperature, indicating only a weak instability of the optical  $\Gamma_{12}$  phonon. In fact, the minima at  $\epsilon \neq 0$  develop *before* the cubic phase becomes unstable with respect to the sublattice distortion at fixed  $\epsilon=0$ . Therefore, we find that the optical  $\Gamma_{12}$  phonon frequency does not tend to zero as  $T$  approaches the cubic-to-tetragonal transition point  $T_M$ , in good agreement with the experimental observation that this frequency softens when approaching the transition but never actually reaches zero, and stiffens again below the transition point.

The predicted temperature dependence of physical quantities is illustrated in Fig. 8, showing the tetragonal strain  $\epsilon_0(T)$ , elastic constant  $C'(T)$ , zone-center optical  $\Gamma_{12}$  phonon frequency  $\nu_{\Gamma_{12}}(T)$ , and equilibrium free energies of the cubic and tetragonal phases. Our results demonstrate that with decreasing temperature the crystal becomes unstable with respect to a combination of the tetragonal strain  $\epsilon$  and sublattice distortion  $\delta$ . In what follows, we show the results for  $c/a < 1$  corresponding to  $\epsilon < 0$ , although the cubic phase is unstable with respect to  $\epsilon > 0$  as well.

Figure 8(a) shows that the cubic  $A_{15}$  phase is stabilized at  $T_M \approx 450$  K, which is ten times larger than the experimentally observed transition temperature,  $T_M^{\text{exp}} \approx 40$  K. The transition is weakly first order [see the discussion of the behavior of  $\epsilon(T)$  and  $C'(T)$ ]. Since the free energy has almost continuous derivative at  $T_M$ , we do not expect a significant latent heat production. The free-energy difference  $F_{\text{cubic}}(T) - F_{\text{tet}}(T)$  becomes smaller than  $k_B T$  at 130 K, suggesting that lattice vibrations should also influence the relative stability of both phases. At present we can only argue that the vibrational entropy should favor the high-symmetry cubic phase and therefore reduce the calculated  $T_M$ . The tetragonality parameter  $\epsilon(T)$ , shown in Fig. 8(b), has a small discontinuity at  $T_M$ , making this transition nearly second order. Similar behavior is seen in the experiments.<sup>39</sup> Fluctuations will presumably increase the first-order character, since they only delay the transition but do not change the underlying energy surface.

We next discuss the temperature-dependent elastic properties of  $\text{Nb}_3\text{Sn}$ . Figure 8(c) demonstrates that the shear elastic constant  $C'(T)$  shows a very pronounced softening as  $T \rightarrow T_M$ , approaches zero at  $T_M$  and then stiffens to a finite value as  $T \rightarrow 0$  in the tetragonal phase. Furthermore  $C'(T) \propto |T - T_M|$  close to  $T_M$ , which is a clear indication of the occurrence of a first-order transition.<sup>7</sup> This is a clear success of the present calculation, since it describes the experimental observations<sup>38</sup> very well.

Another quantity of interest is the temperature dependence of the optical  $\Gamma_{12}$  phonon frequency:

$$\nu_{\Gamma_{12}}(T) = \frac{1}{2\pi} \sqrt{\frac{F_{\delta, \delta}(T)}{M^* a_0^2}}, \quad (14)$$

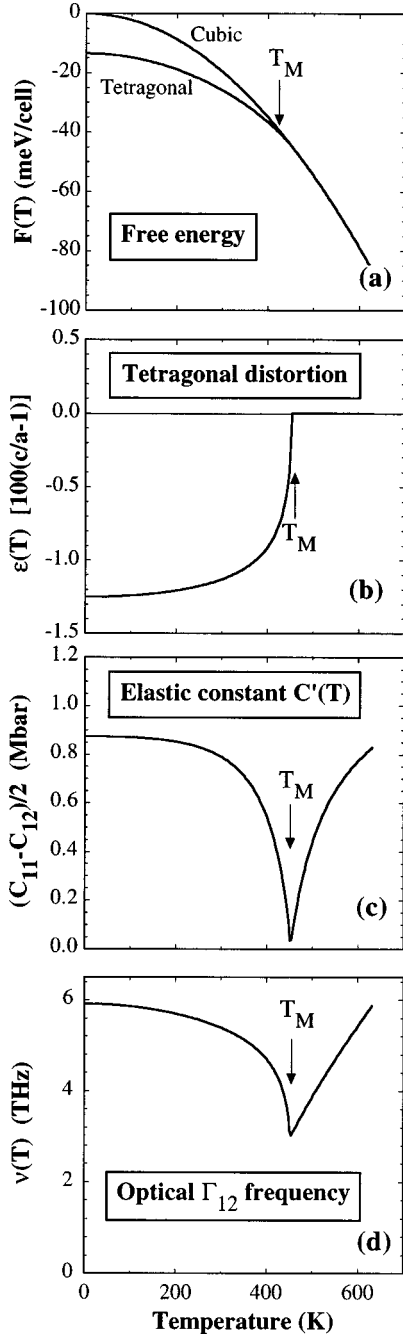


FIG. 8. The calculated temperature dependent physical properties of  $\text{Nb}_3\text{Sn}$ .

where  $M^* = 4M_{\text{Nb}}$  is the effective mass of the mode and  $a_0$  is the equilibrium lattice parameter. Due to the large  $\delta$  dependence of  $\gamma(\epsilon, \delta)$ , it is expected that  $\nu_{\Gamma_{12}}(T)$  will show a strong temperature dependence. Figure 8(d) illustrates that this is indeed the case. It is rewarding to see that the frequency does not approach zero at the transition point, which has been explained above in the discussion of Fig. 7. This is also consistent with the conclusion of Miller and Axe<sup>40</sup> that it is impossible for the frequency of a Raman-active mode (like  $\nu_{\Gamma_{12}}$ ) to go to zero without first producing an elastic instability of the crystal.

## V. DISCUSSION

Based on first-principles LDA total-energy and free-energy calculations, we have ascribed the anomalous structural properties of  $\text{Nb}_3\text{Sn}$  to a low-temperature structural instability of the cubic A15 phase. The effects of the electronic excitations on the structural stability and cubic-to-tetragonal phase transition have been studied by using the finite- $T$  Fermi-Dirac distribution function, noninteracting electronic entropy Eq. (3), and LDA  $T=0$  exchange and correlation energy functional. Phonon excitations and electron-phonon interactions have been excluded from this simple picture, although there is good reason to suspect that they should play an important role in this system. In what follows we discuss what are the successes and failures of this simple approach, and what are the implications for more refined theoretical treatments of the structural transitions in A15 compounds.

Several qualitative features of the structural phase transition are reproduced correctly:

(i) The cubic phase is stable at elevated temperatures, and spontaneously distorts tetragonally at low temperatures.

(ii) The transition develops negligible latent heat as well as small discontinuity in the tetragonality parameter  $\epsilon(T)$ , which makes it appear as nearly second order.

(iii) The elastic constant  $C'(T)$  tends to 0 as  $T \rightarrow T_M^+$  [in fact,  $C'(T) \propto T - T_M$ ], and then stiffens rapidly as  $T \rightarrow 0$ . It has a discontinuous derivative at  $T_M$ .

(iv) The frequency of the optical  $\Gamma_{12}$  phonon decreases as  $T \rightarrow T_M$ , but never actually reaches zero. It stiffens again below the transition temperature.

Taking into account the simplicity of the present model, it is not surprising that the calculated transition temperature is  $T_M^{\text{calc}} = 450$  K, while experimentally  $T_M \approx 40$  K. There are several possible causes for this discrepancy. First, the electron-phonon interaction has been completely neglected. More refined treatments should attempt to include finite lifetime and nonadiabatic effects on the states at the Fermi surface. Whether they would lead to an increase in the effective temperature for the electrons at the Fermi level is an open question which can only be settled by further studies. Second, the experimental samples are known to contain a substantial fraction of crystal defects. It is difficult to predict how these defects affect the behavior of  $\text{Nb}_3\text{Sn}$ , although it has been speculated<sup>1,3</sup> that they would somewhat smear out the sharp features in the electronic structure. And finally, anharmonic effects should also be important at low temperatures, since the calculated energy barrier at  $T=0$  K between the local minima at  $\delta < 0$  and  $\delta > 0$  when  $\epsilon=0$  is only 4–5 meV/cell, which is of the same magnitude as  $k_B T_M$ . We have demonstrated that these anharmonicities do not survive at elevated temperatures where the electronic excitations stabilize the cubic phase and the  $\Gamma_{12}$  optical phonon is both stable and harmonic. In conclusion,  $\text{Nb}_3\text{Sn}$  exhibits a subtle interplay between the vibrational and electronic excitations, and the present calculations strongly suggest that a complete theory of the unusual properties of A15 compounds should include both.

## ACKNOWLEDGMENTS

This work was supported by the Swedish research councils NFR, TFR, and NUTEK.

- \*Present address: National Renewable Energy Laboratory, Golden, CO 80401.
- <sup>1</sup>L. R. Testardi, *Rev. Mod. Phys.* **47**, 637 (1975).
  - <sup>2</sup>M. Weger and I. B. Goldberg, in *Solid State Physics: Advances in Research and Applications*, edited by H. Ehrenrich, F. Seitz, and D. Turnbull (Academic, New York, 1973), Vol. 28.
  - <sup>3</sup>P. B. Allen, in *Dynamical Properties of Solids*, edited by G. K. Horton and A. A. Maradudin (North-Holland, Amsterdam, 1980), Vol. 3.
  - <sup>4</sup>B. W. Batterman and C. S. Barrett, *Phys. Rev. Lett.* **13**, 390 (1964).
  - <sup>5</sup>R. Mailfert, B. W. Batterman, and J. J. Hanak, *Phys. Lett.* **24A**, 315 (1967).
  - <sup>6</sup>K. R. Keller and J. J. Hanak, *Phys. Rev.* **154**, 628 (1967).
  - <sup>7</sup>P. W. Anderson and E. I. Blount, *Phys. Rev. Lett.* **14**, 217 (1965).
  - <sup>8</sup>G. Shirane and J. D. Axe, *Phys. Rev. B* **4**, 2957 (1971).
  - <sup>9</sup>Y. Fujiii, G. Shirane, J. B. Hastings, Y. Inada, and N. Kitamura, *Bull. Am. Phys. Soc.* **26**, 478 (1981); Y. Fujiii, J. B. Hastings, M. Kaplan, G. Shirane, Y. Inada, and N. Kitamura, *Phys. Rev. B* **1**, 364 (1982).
  - <sup>10</sup>L. R. Testardi, T. B. Batterman, W. A. Reed, and V. G. Chirba, *Phys. Rev. Lett.* **15**, 250 (1965).
  - <sup>11</sup>J. Labbe and J. J. Friedel, *J. Phys. (Paris)* **27**, 153 (1966).
  - <sup>12</sup>R. W. Cohen, C. D. Cody, and J. J. Halloran, *Phys. Rev. Lett.* **19**, 840 (1967).
  - <sup>13</sup>L. P. Gorkov, *Zh. Eksp. Teor. Fiz. Pis'ma Red.* **17**, 525 (1973) [*JETP Lett.* **17**, 379 (1973)]; *Zh. Eksp. Teor. Fiz.* **65**, 1658 (1973) [*Sov. Phys. JETP* **38**, 830 (1974)]; L. P. Gorkov and O. N. Dorokhov, *J. Low Temp. Phys.* **22**, 1 (1976); *Zh. Eksp. Teor. Fiz. Pis'ma Red.* **21**, 656 (1975) [*JETP Lett.* **21**, 310 (1975)].
  - <sup>14</sup>R. N. Bhatt, *Phys. Rev. B* **16**, 1915 (1977).
  - <sup>15</sup>T. K. Lee, J. L. Birman, and S. J. Williamson, *Phys. Rev. Lett.* **39**, 839 (1977); (a) T. K. Lee, J. L. Birman, and S. J. Williamson, *Phys. Lett.* **64A**, 89 (1977).
  - <sup>16</sup>L. R. Testardi, *Phys. Rev. B* **5**, 4342 (1972).
  - <sup>17</sup>L. F. Mattheiss, *Phys. Rev. B* **8**, 3719 (1975).
  - <sup>18</sup>B. M. Klein, D. A. Papaconstantopoulos, and L. L. Boyer, *Ferroelectrics* **16**, 299 (1977).
  - <sup>19</sup>B. M. Klein, L. L. Boyer, D. A. Papaconstantopoulos, and L. F. Mattheiss, *Phys. Rev. B* **18**, 6411 (1978).
  - <sup>20</sup>B. M. Klein, L. L. Boyer, and D. A. Papaconstantopoulos, *Phys. Rev. Lett.* **42**, 530 (1979).
  - <sup>21</sup>T. Jarlborg and G. Arbman, *J. Phys. F* **7**, 1635 (1977).
  - <sup>22</sup>L. F. Mattheiss and W. Weber, *Phys. Rev. B* **25**, 2248 (1982); W. Weber and L. F. Mattheiss, *ibid.* **25**, 2270 (1982).
  - <sup>23</sup>P. Hohenberg and W. Kohn, *Phys. Rev.* **136**, 864 (1964); W. Kohn and L. J. Sham, *Phys. Rev. A* **136**, 1133 (1965).
  - <sup>24</sup>J. P. Perdew and A. Zunger, *Phys. Rev. B* **23**, 5048 (1981).
  - <sup>25</sup>D. M. Ceperley and B. J. Alder, *Phys. Rev. Lett.* **45**, 566 (1980).
  - <sup>26</sup>L. Kleinman and D. M. Bylander, *Phys. Rev. Lett.* **48**, 1425 (1982); P. E. Blöchl, *Phys. Rev. B* **41**, 5414 (1990); D. Vanderbilt, *ibid.* **41**, 7892 (1990).
  - <sup>27</sup>S. Louie, S. Froyen, and M. L. Cohen, *Phys. Rev. B* **26**, 1738 (1982).
  - <sup>28</sup>V. Ozoliņš, Ph.D. thesis, Royal Institute of Technology, Sweden, 1996.
  - <sup>29</sup>A. M. Rappe, K. M. Rabe, E. Kaxiras, and J. D. Joannopoulos, *Phys. Rev. B* **41**, 1227 (1990).
  - <sup>30</sup>K.-M. Ho, C.-L. Fu, B. N. Harmon, W. Weber, and D. R. Hamann, *Phys. Rev. Lett.* **49**, 673 (1982); C.-L. Fu and K.-M. Ho, *Phys. Rev. B* **28**, 5480 (1983).
  - <sup>31</sup>M. Methfessel and A. T. Paxton, *Phys. Rev. B* **40**, 3616 (1989).
  - <sup>32</sup>M. J. Gillan, *J. Phys.: Condens. Matter* **1**, 689 (1989).
  - <sup>33</sup>P. E. Blöchl, O. Jepsen, and O. K. Andersen, *Phys. Rev. B* **49**, 16 223 (1994).
  - <sup>34</sup>G. R. Johnson and D. H. Douglass, *J. Low Temp. Phys.* **14**, 565 (1974).
  - <sup>35</sup>N. D. Mermin, *Phys. Rev.* **137**, A1441 (1965).
  - <sup>36</sup>N. W. Ashcroft and N. D. Mermin, *Solid State Physics* (Saunders College, Philadelphia, 1976).
  - <sup>37</sup>Z. W. Lu and B. M. Klein, *Phys. Rev. Lett.* **79**, 1361 (1997).
  - <sup>38</sup>W. Rehwald, M. Rayl, R. W. Cohen, and G. D. Cody, *Phys. Rev. B* **6**, 363 (1971).
  - <sup>39</sup>R. Mailfert, B. W. Batterman, and J. J. Hanak, *Phys. Status Solidi* **32**, K67 (1969).
  - <sup>40</sup>P. B. Miller and J. D. Axe, *Phys. Rev.* **163**, 924 (1967).